J Dent Res 74(12):1891-1898, December, 1995

HeNe-Laser Light Scattering by Human Dental Enamel

J.R. Zijp, J.J. ten Bosch, and R.A.J. Groenhuis[1]

Laboratory for Materia Technica, State University of Groningen, Bloemsingel 10, 9712 KZ Groningen, The Netherlands; [1]present address, Moeflonstraat 44, 6531 JP Nijmegen, The Netherlands

Abstract. Knowledge of the optical properties of tooth enamel and an understanding of the origin of these properties are necessary for the development of new optical methods for caries diagnosis and the measurement of tooth color. We measured the scattering intensity functions for HeNe-laser light of 80- to 100-µm-thick human dental enamel slabs. The asymmetry factors were calculated to be g = 0.68 at 633 nm. By measuring the collimated beam attenuation, we determined the scattering coefficient to be s = 6.6 mm^{-1}. From Fraunhofer diffraction patterns, obtained from transmission of the laser beam, we calculated the periodicity of the prismatic structure as 5.4 µm. We present a model containing scattering by crystals and by prisms. It shows that the prisms are the most important scatterers but that the crystals are responsible for the back-scattering.

Key words: lasers, optical properties, light-scattering, human enamel.

Received April 4, 1995; Accepted September 19, 1995

Introduction

Studying the optical properties of dental materials is necessary to extend the knowledge of the processes and structures that cause the color of teeth. The outer surface of a tooth crown consists of enamel. Sound enamel is nearly transparent. Its light-scattering coefficient for fluxes, S, decreases from 9 to 1.5 mm^{-1} at increasing wavelengths from 400 to 700 nm. The absorption coefficient for fluxes, K, equals 0.1 mm^{-1} over this wavelength region (Spitzer and ten Bosch, 1975). Recently, the asymmetry factor for single scattering, g = 0.68 ± 0.09, was obtained from experiments with a thick enamel sample, assuming a Henyey-Greenstein angular intensity function (Vaarkamp *et al.*, 1995).

By fitting linear combinations of isotropic and Henyey-Greenstein angular intensity functions, we can calculate much lower values of the asymmetry factors g (Fried *et al.*, 1995). The angular intensity function used in this method is given by:

$$E(\theta) = f_d + (1 - f_d)\left[\frac{(1 - g^2_{HG})}{(1 + g^2_{HG} - 2\,g_{HG}\cos\theta)^{3/2}}\right] \quad (1)$$

with f_d, a fit parameter, expressing the isotropic contribution with respect to the Henyey-Greenstein part, and g_{HG}, the asymmetry factor of the Henyey-Greenstein intensity function.

The reported values are g_{HG} = 0.96 (at all three wavelengths used), f_d = 0.35 (at wavelengths of 1053 and 632 nm), and f_d = 0.60 (at 543 nm). This results in total asymmetry factors g = 0.462 (at 1053 and 632 nm) and g = 0.240 (at 543 nm).

Fraunhofer diffraction of light can be observed from thin enamel samples (O'Brien, 1988). Two-dimensional Fraunhofer patterns can be used to determine the distribution of the values of the periodicity of the structure of prisms and the interfaces between them (Zijp and ten Bosch, 1995). The fluorescence properties of tooth enamel have been well-

reviewed (Hefferren *et al.*, 1971; Scharf, 1971).

Better understanding of the optical properties of dental enamel requires knowledge of its single-scattering properties, *i.e.*, the scattering coefficients for collimated light, *s*, and single-scattering intensity functions, $E(\theta)$. These should be measured from thin samples. We present such data in this paper and compare them with theoretical predictions. Preliminary results have been published (Groenhuis, 1981).

Materials and methods

Theoretical calculations

To understand the light-scattering properties of biological tissues, we must consider the structures within these materials. The main structures in human dental enamel are the mineral crystals and the keyhole-shaped prisms in which they are organized. We shall consider these structures and their effects on the scattering properties separately.

Scattering by crystals. Human dental enamel consists 87 vol% of natural hydroxyapatite (HAP) crystals (Arends and ten Cate, 1981), with the balance water and organic material, mainly proteins. The HAP crystals are hexagonal cylinders with the following dimensions: thickness = 25 nm, width = 40 nm, and length = 160 nm (Scott and Symons, 1971). Other investigators have found that the lengths can vary over wide ranges (from 100 to 1000 nm, Jongebloed and Molenaar, 1975; from 21 to 10,000 nm, Rönnholm, 1962). Using the dimensions found by Scott and Symons, the average crystal volume is 1.3×10^{-22} m^3, and we find the number of crystals to be $N_c \simeq 6.7 \times 10^{21}$ m^{-3} in enamel. The refractive index for visible light of HAP crystals is 1.651 (McConnell, 1973), and that of whole enamel is 1.62 (Spitzer and ten Bosch, 1975). From the mineral content of whole enamel, we can calculate its refractive index (*cf.* Appendix 1).

To calculate the light-scattering intensity function, we estimated the role of the crystals by assuming a circular cross-section and a random orientation overall (see Appendix 2).

Scattering by prisms. In enamel, the crystals are organized in keyhole-shaped prisms. These prisms are 4 to 6 μm wide and extend from the dentin-enamel junction to the outer surface of the tooth. Schematic drawings of the prisms (*e.g.*, Griebstein, 1965) and photographs have been published (Zelander, 1973); similar figures can be found in many textbooks dealing with dental tissues. When the keyhole is divided into a head and a tail, the crystals within the head are oriented nearly parallel to the axis of the prism, and those within the tail are oriented nearly perpendicular to the prism axis (Griebstein, 1965). From a photograph (Zelander, 1973), we determined the geometric cross-sections (*i.e.*, perpendicular to their principal axes) of the prisms to be about 4.0×10^{-11} m^2.

Between the prisms, there is an interprismatic area with an average thickness of about 0.1 μm (Arends and ten Cate, 1981). One can estimate the average geometric cross-section of interprismatic substance by measuring its average area per prism on the photograph (Zelander, 1973); this is about 1.5×10^{-12} m^2. Assuming that the volume fractions are equal to the cross-section fractions, the prism volume fraction can be estimated as $f_p = 0.96$. The number of prisms *per* unit volume was estimated as $N_p \simeq 2.4 \times 10^{13}$ m^{-3}, based on a length of 1 mm.

In the interprismatic area, the crystal orientation is random, leading to a lower mineral content and a higher content of water and organic material. To estimate the mineral volume fraction in the interprismatic material, we filled a glass box with pencils which were also randomly distributed. The dimensions of the pencils were of the same proportion as those of the crystals. The dimensions of the box were much larger than the dimensions of the pencils. The volume fraction of the pencils appeared to be almost 0.70. We took this value as an estimation of the mineral volume fraction in the interprismatic area. Since the mineral volume fraction in whole enamel is about 0.87 (Arends and ten Cate, 1981), we estimated it as 0.88 in the prisms.

Calculation of the indices of refraction of the prisms and the interprismatic substance appears in Appendix 1.

In our measurement set-up, we observed the prisms at angles $\alpha = 20°\text{-}90°$ and $\varnothing = 60°\text{-}90°$ (with α and $\varnothing$ as defined by van de Hulst, 1981). Because the measured angular intensity functions did not show systematic differences on the site in the tooth where the slab was cut, we estimated a mean angular intensity function $E(\theta)$ of an ensemble of cylinders by averaging these intervals of α and $\varnothing$. More details about the calculation of the angular intensity function are given in Appendix 3.

Diffraction by prisms. In enamel, the structure of prisms and interprismatic substance can be considered as a grating. The width of the prisms shows some variation, and the prisms are somewhat curved and not exactly aligned. We consider this as a grating with an irregular periodicity and curved slits. The irregular periodicity will cause an interference pattern with a sharp principal maximum, a wide first-order maximum, and vanishing higher-order maxima. The curvature will cause spreading of the first-order maxima around the principal axis. Calculations on the diffraction pattern are explained in Appendix 4.

Experiments

Samples. We used 6 extracted human third molars. From each molar, 5 slabs with a thickness of from 80 to 100 μm were cut, parallel to the buccal surface. They were stored on wet tissues in a refrigerator until measurements were performed.

Measurements. The angular intensity functions were measured with equipment as described previously (Zijp and ten Bosch, 1991). In the present measurements, however, the scattering cells contained a solution which matched the refractive index of enamel. This solution was made of a saturated solution of potassium-iodine (KI) in water, to which mercury-iodine (HgI_2) was added until the refractive index of the solution was 1.62, and so matched the refractive index of enamel. We used a tunable HeNe laser (LSTPC-1010, PMS Electro Optics, Boulder, CO) at wavelengths (and powers) of 632.8 nm (4 mW), 594.1 nm (0.6 mW), and 543.5 nm (0.3 mW). We measured the angular intensity functions in the planes parallel and perpendicular to the tooth axis. From the measured angular intensity functions parallel to the tooth axes, the asymmetry factors for scattering, *g*, were calculated by:

$$g = \frac{\int_{0°}^{180°} E(\theta) \cos\theta \sin\theta \, d\theta}{\int_{0°}^{180°} E(\theta) \sin\theta \, d\theta} \qquad (2)$$

We consider the Fraunhofer diffracted light as unscattered light, and so the undiffracted angular intensity functions, *i.e.*, those measured parallel to the prisms, should be used for calculating g.

In practice, it is impossible to calibrate the measurement of $E(\theta)$ with respect to the incident beam power E_0. Therefore, the scattering coefficient s was determined from the attenuation (by scattering) of the incident beam. Thus, we measured the transmission T at $\theta = 0°$ at the laser wavelength of 632.8 nm. The mean thickness t of each slab was calculated from 5 measurements with a micrometer. The measured scattering coefficient was calculated by: $s_m = -\ln(T)/t$. The absorption coefficient was assumed to be much smaller than the scattering coefficient (Spitzer and ten Bosch, 1975).

The Fraunhofer diffraction patterns were measured with 6 other slabs from 6 teeth prepared and stored as described. The measuring set-up is shown schematically in Fig. 2. We used a HeNe laser at 632.8 nm. The diffracted radiation was mirrored by a glass plate on a spectralon block (Labsphere, North Sutton, NH). This pattern was imaged by means of a M 1430-P CCD camera (EG&G-Par, Princeton, NJ), coupled to a computer by a 14-bit analog-to-digital converter. The images measured 300 x 300 pixels, and were taken without and with neutral density filters of 10%, 1%, 0.1%, and 0.01% transmission in the incident beam. These pictures showed different degrees of saturation of CCD-camera pixels, and were combined to yield an intensity profile with a dynamic range of 6 orders of magnitude, without saturation. The form of such an intensity profile is shown schematically in Fig. 3, in which the density of the dark spots represents the light intensity.

From these images, we calculated the light power P, transmitted in the sectors 1 and 2 (*cf.* Fig. 3), as a function of the angular deviation from the central spot, $\theta = 0°$. This resulted in $P_1(\theta)$ and $P_2(\theta)$. By performing the calculations as set out in Appendix 4, we could predict $P_2(\theta)$ curves for appropriate values of the mean periodicity of the prism structure, d_{mean}, and its standard deviation, σ_d. The curve $P_3(\theta)$ that best fit the experimental result, $P_2(\theta)$, was used to determine d_{mean} and σ_d.

The measured diffraction patterns were further used to determine the angular distribution of the prisms. We calculated the total amount of transmitted light, $P_w(\varnothing)$, in the windows covering the first-order maxima (Fig. 3) as a function of the angle ø.

Results

Calculations

Fig. 1 shows the light-scattering intensity function for a single crystal, multiplied by N_c (dashed line). Calculation of the scattering cross-section of each crystal (at a wavelength of 633 nm, Appendix 2) gives $C_{sca} \simeq 1.4 \times 10^{-19}$ m^2. The number of crystals and their scattering cross-section determine the linear scattering coefficient, $s_c = N_c \times C_{sca} \simeq 0.94$ mm^{-1}. This

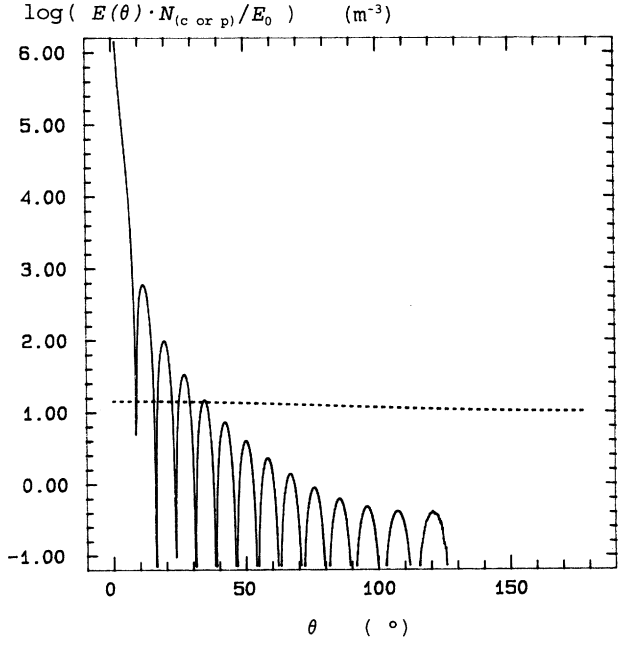

Figure 1. Calculated angular intensity functions. Dashed line for randomly oriented cylinders as a model for the mineral crystals. Solid line for oriented cylinders as a model for the prisms. The ordinate value expresses the irradiance at the detector per unit irradiance of the incident beam per volume irradiated enamel (in m^3), where the detector is positioned in a direction u with respect to the incident direction.

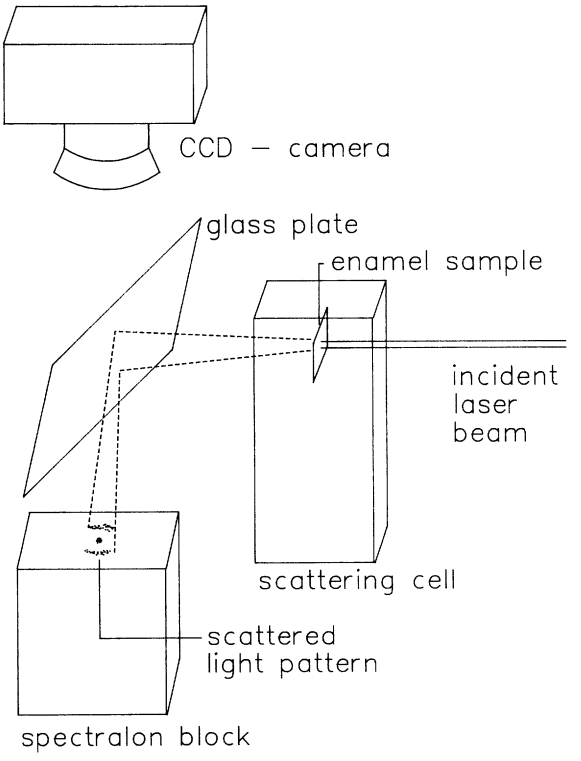

Figure 2. Set-up for measurement of the Fraunhofer diffraction pattern.

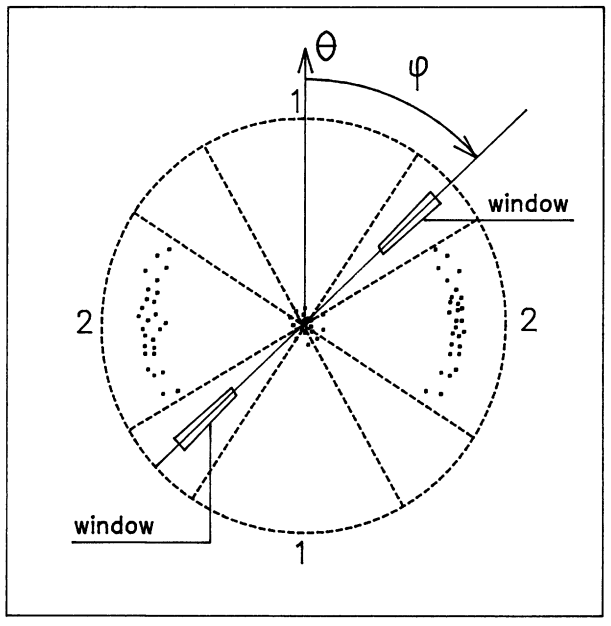

Figure 3. Schematic example of a measured Fraunhofer diffraction pattern. The black dot density represents the light intensity. The incident beam is a thin pencil beam in the center of the picture. The sectors numbered 1 and 2 are used to calculate the functions $P_1(\theta)$ and $P_2(\theta)$, respectively. The windows at angle ø are used to calculate $P_w(ø)$.

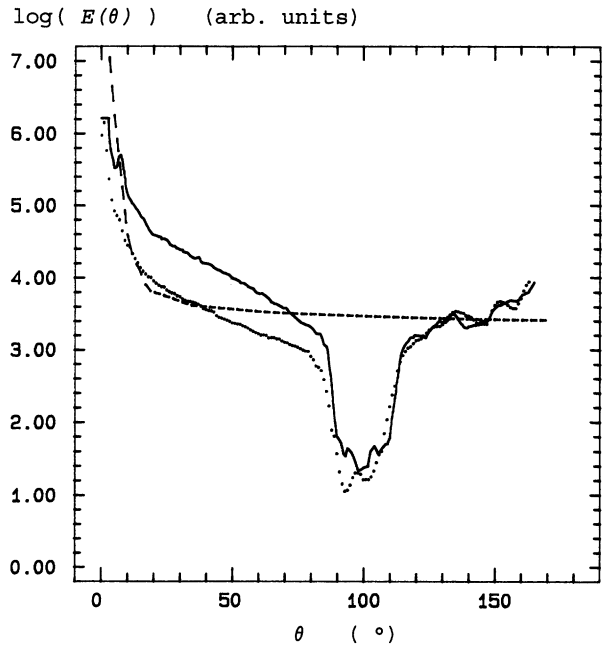

Figure 4. Typical examples of angular intensity functions of enamel at 633 nm. Full and dotted lines: measured with the scattering plane perpendicular and parallel to the tooth axis, respectively. Dashed line: calculated perpendicular to the tooth axis.

coefficient is proportional to the estimated lengths of the model crystals (so far assumed as 160 nm), because N_c is proportional to the inverse of their lengths, and C_{sca} is proportional to the square of their lengths.

The angular intensity function for a single prism, multiplied by N_p, is shown in Fig. 1 as the solid line. The scattering cross-section for each prism is estimated as $C_{sca} \simeq 2.4 \times 10^{-10}$ m^2 (at a wavelength of 633 nm, Appendix 3). Calculations with different prism lengths showed that C_{sca} is almost proportional with the length of the model prism.

The number of prisms and their scattering cross-section determine the corresponding scattering coefficient, which can be estimated as $s_p = N_p \times C_{csa} \simeq 5.8$ mm^{-1}. This scattering coefficient is independent of the lengths of the model crystals.

Experiments

When the thin enamel slabs are observed in daylight, they appear to be pale blue in reflection and pale yellow in transmission.

Typical examples of measured angular intensity functions are shown in Fig. 4. The calculated asymmetry factors, g, from these functions are shown in the Table.

From 55 measurements (of 11 samples) of the transmission at $\theta = 0°$, we found $s_m = 6.6 \pm 2.7$ mm^{-1}.

Typical examples of the diffraction patterns as a function of the diffraction angle θ are given as $P_1(\theta)$ and $P_2(\theta)$ in Fig. 5. Predicted curves $P_3(\theta)$ were fitted to the $P_2(\theta)$ curves. By doing so, from 6 measurements on 6 samples, we found overall mean values of $d_{mean} = 5.4$ µm and $\sigma_d = 1.0$ µm. The fit corresponding to $P_2(\theta)$ is also shown in Fig. 5.

Fig. 6 shows $P_w(ø)$ for one of the samples. It illustrates the distribution of the curvature or misalignment of the prisms. We found the full width at half-maximum (FWHM) of all 6 measured distributions to be $\Delta ø = 74° \pm 11°$.

Table. Asymmetry factors, g, of enamel

Wavelength (nm)	n[a]	Mean ± S.D.[b]
633	9	0.68 ± 0.10
594	4	0.68 ± 0.20
543	4	0.74 ± 0.23

[a] Some samples were broken after measurement at 633 nm.
[b] Standard deviation includes variation among the samples.

Discussion

The observation that the slabs look blueish in reflection and yellowish in transmission leads to the conclusion that structures smaller than the wavelength of light play a considerable role in the light-scattering process. This is supported by the measured asymmetry factors, g (Table), because structures as small as the mineral crystals would cause low asymmetry factors, $g \simeq 0$, and those as large as the prisms would cause high asymmetry factors, $g \simeq 1$ (Fig. 1). The measured g values are between these values. The g value we measured at 633 nm is equal to that found previously by a different method (Vaarkamp *et al.*, 1995). Our measured g values deviate significantly from those found by the fitting procedure (Fried *et al.*, 1995). This procedure has the disadvantage that the addition of a small isotropic fraction to the resulting intensity function will

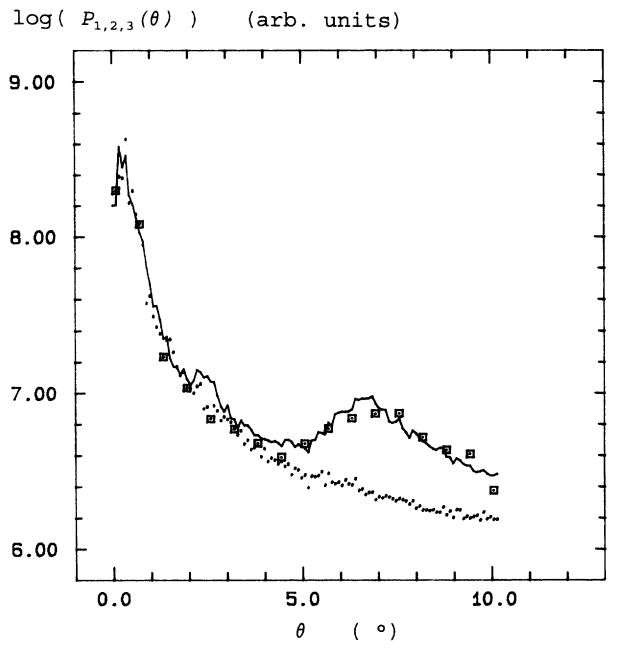

Figure 5. Typical example of the measured reflected power $P_1(\theta)$ (solid line) in sector 1, $P_2(\theta)$ (dotted line) in sector 2, and $P_3(\theta)$ (squares) fitted curve, as a function of the angle θ.

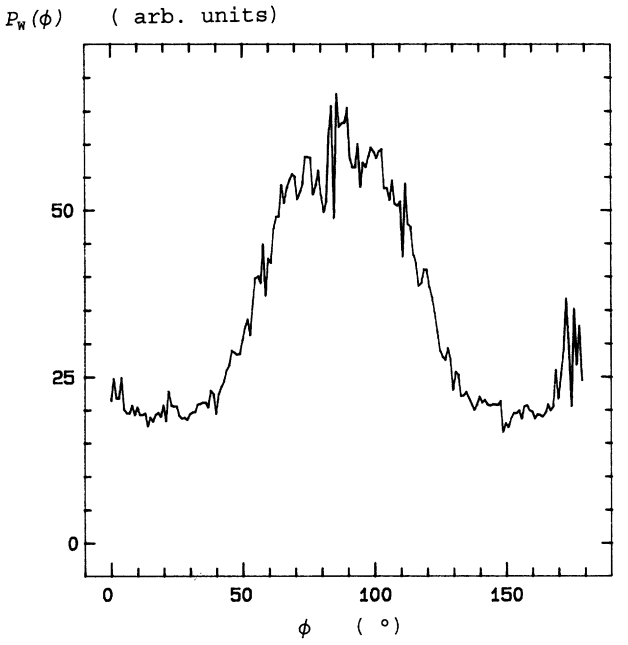

Figure 6. Typical example of the measured reflected power in the windows $P_w(\phi)$ as a function of the angle ø.

result in a large reduction in the calculated g value. This is a consequence of the fact that the Henyey-Greenstein intensity functions are peaked very sharply forward. We observed an increase in the standard deviation of the measured g values with decreasing wavelength, which is due to decreasing laser power. Therefore, we were unable to determine the increase of g with decreasing wavelength that is theoretically expected.

The measured angular intensity function (Fig. 4) shows a minimum around 90°, caused by the shade cast by the sample-holder. We expected the true angular intensity function to have, at the minimum, a smooth form, but not one so deep (between 80 and 120°). By adding and smoothing both theoretical functions of Fig. 1, we will get an intensity function peaked sharply forward. We expect that the resonances will vanish in practice, because the prisms are not uniform, since the crystals within them are somewhat oriented. Also, the prisms do not have a circular cross-section, as do the cylinders in the model.

The calculated linear scattering coefficient, s, can be found by adding those found from the calculations for scattering by mineral crystals and prisms. We found $s = 6.7$ mm^{-1}. It should be noted that this result is not dependent upon the length of the modeled prisms. This value matches the measured value, $s_m = 6.6 \pm 2.4$ mm^{-1}.

Adding the functions shown in Fig. 1 results in an angular scattering intensity function which shows too little back-scattering. This back-scattering can be introduced by assuming stronger scattering from the crystals, which can be obtained by assuming longer crystals than in the model presented in Appendix 2. This assumption would be in agreement with reports on very long crystals (Orams *et al.*, 1974; Daculsi *et al.*, 1984), which are fractured in the preparation of the samples. If we thus assume the scattering from the crystals to be stronger by a factor of 10, the theoretical curve obtained will better match the measured one (*cf.* Fig. 4, dashed line). This procedure, however, leads to a scattering coefficient which would be too high. This theoretical curve does not show back-scattering as strong as those measured, probably caused by reflectance of the forward-scattered radiation at the solution-glass and glass-air surfaces of the scattering cell.

The values of d_{mean} (5.4 μm) and σ_d (1.0 μm) compare well with other measurements of the diameters of enamel prisms (Zelander, 1973).

The data presented are all from third molars. Since it has been shown that the scattering coefficient of enamel is weakly correlated to tooth color (ten Bosch and Coops, 1995), it may be expected that the scattering in enamel of teeth with usually darker color, *e.g.*, cuspids, is different.

If the enamel samples were cut in other orientations, *e.g.*, perpendicular to the surface, this would affect the measured and calculated optical parameters. In that case, we would expect lower scattering coefficients, because waveguide effects will play a considerable role (Altshuler and Grisimov, 1989).

Acknowledgments

This work was supported by the University of Groningen.

The authors wish to thank Mrs. H. Middel and Dr. F.K.L. Spijkervet of the Department of Oral and Maxillofacial Surgery of the Academic Hospital Groningen for providing the extracted molars.

References

Altshuler GB, Grisimov VN (1989). New optical effects in the human hard tissues. *SPIE* 1353:97-101.

Arends J, ten Cate JM (1981). Tooth enamel remineralization. *J Crystal Growth* 53:135-147.

Born MA, Wolf E (1980). Principles of optics. 6th ed. Oxford: Pergamon Press, p. 404.

Daculsi G, Menanteau J, Kerebel LM, Mitre D (1984). Length and shape of enamel crystals. *Calcif Tissue Int* 36:550-555.

Emslie AG, Aronson JR (1973). Spectral reflectance and emittance of particulate materials. 1: Theory. *Appl Opt* 12:2563-2572.

Fried D, Glena RE, Featherstone JDB, Seka W (1995). Nature of light scattering in dental enamel and dentin at visible and near-infrared wavelengths. *Appl Opt* 34:1278-1285.

Griebstein WJ (1965). Discussion of fourth session. In: Tooth enamel. Stack MV, Fearnhead RW, editors. Bristol: John Wright & Sons Ltd, p. 191.

Groenhuis RAJ (1981). Scattering and absorption of light by turbid materials, especially dental enamel (dissertation). Groningen, The Netherlands: State Univ. of Groningen.

Hefferren JJ, Hall JB, Bennet E (1971). Luminescence as a tool to study enamel interactions. In: Tooth enamel II. Fearnhead RW, Stack MV, editors. Bristol: John Wright & Sons Ltd, pp. 161-165.

Jongebloed WL, Molenaar I, Arends J (1975). Morphology and size-distribution of sound and acid-treated enamel crystallites. *Calcif Tissue Res* 19:109-123.

McConnell D (1973). Apatite. Its crystal chemistry, mineralogy, utilization, and geologic and biologic occurrences. New York: Springer-Verlag.

O'Brien WJ (1988). Fraunhofer diffraction of light by human enamel. *J Dent Res* 67:484-486.

Orams HJ, Phakey PP, Rachinger WA, Zybert JJ (1974). Visualisation of micropore structure in human dental enamel. *Nature* 252:584-585.

Rönnholm E (1962). The amelogenesis of human teeth as revealed by electron microscopy. II. The development of the enamel crystallites. *J Ultrastruct Res* 6:249-303.

Scharf F (1971). On the natural luminescence of the hard tissues of tooth enamel and dentin (in German). *Stoma* (Heidelb) 24:10-25.

Scott FR, Symons NBB (1971). Introduction to dental anatomy. 6th ed. Edinburgh and London: Livingstone.

Spitzer D, ten Bosch JJ (1975). The absorption and scattering of light in bovine and human dental enamel. *Calcif Tissue Res* 17:129-137.

ten Bosch JJ, Coops JC (1995). Tooth color and reflectance as related to light scattering and enamel hardness. *J Dent Res* 74:374-380.

Vaarkamp J, ten Bosch JJ, Verdonschot EH (1995). Propagation of light through human dental enamel and dentine. *Caries Res* 29:8-13.

van de Hulst HC (1981). Light scattering by small particles. New York: Dover Publications.

Zelander T (1973). The enamel. In: Histology of the human tooth. Mjör IA, Pindborg JJ, editors. Copenhagen: Munksgaard.

Zijp JR, ten Bosch JJ (1991). Angular dependence of HeNe-laser light scattering by bovine and human dentine. *Arch Oral Biol* 36:283-289.

Zijp JR, ten Bosch JJ (1995). Two dimensional patterns of Fraunhofer diffraction by dental enamel. *SPIE* 2626: 113-120.

Appendix 1. Calculation of the refractive indices of the prisms, the interprismatic area, and whole enamel

The refractive index of a whole substance composed of surrounding material and particles with a different refractive index can be calculated by (Emslie and Aronson, 1973):

$$\bar{n} = n_s \sqrt{1 + \frac{2_p\left[\left[\frac{n_p^2}{n_p^2 - n_s^2}\right]\ln\left[\frac{n_p}{n_s}\right]^2 - 1\right]}{1 - f_p + \frac{2f_p n_s^2}{n_p^2 - n_s^2}\left[\left[\frac{n_p^2}{n_p^2 - n_s^2}\right]\ln\left[\frac{n_p}{n_s}\right]^2 - 1\right]}} \quad (3)$$

with:

$\bar{n}$ as the refractive index of the substance,

n_p as the refractive index of the particles, *i.e.*, the mineral crystals = 1.651 (McConnell, 1973),

n_s as the refractive index of the surrounding material, *i.e.*, proteins and water = 1.40 (estimated), and

f_p as the volume fraction of the particles in the substance.

We can use Eq. 3 to calculate the refractive index of the prisms. With $f_p = 0.88$, being the volume fraction of mineral crystals in the prisms, we find $\bar{n}_{prism} = 1.619$.

The refractive index of the interprismatic substance can be found: With $f_p = 0.70$, being the volume fraction of mineral crystals in the interprismatic area, we find $\bar{n}_{int.pr.} = 1.573$.

Applying the same method for whole enamel with $f_p = 0.87$, being the volume fraction of mineral crystals in whole enamel, we find $\bar{n}_{enamel} = 1.616$. This value compares with the measured value of 1.62 (Spitzer and ten Bosch, 1975).

Appendix 2. Calculation of the single-scattering properties of the mineral crystals.

In this calculation, we assume that, for this treatment, the mineral crystals can be considered as randomly oriented circular cylinders. Their scattering properties can be calculated by the Rayleigh-Gans theory (van de Hulst, 1981, p. 98), because both its constraints are fulfilled:

$$\left|\frac{n_{particle}}{\bar{n}} - 1\right| << 1 \qquad \text{and} \qquad ka\bar{n}\left|\frac{n_{particle}}{\bar{n}} - 1\right| << 1 \quad (4)$$

with

$n_{particle}$ as the refractive index of the particles (mineral crystals) = 1.651,

$\bar{n}$ as the refractive index of the environment of the particles (whole enamel) = 1.616,

a as the "radius" of the mineral crystals = 17 nm, and

k as the wavenumber of the light = 9.93×10^6 m^{-1} (at a wavelength of 633 nm, in vacuum).

The angular intensity function for this approximation, with the extra constraint that $ka << 1$, is given by (van de Hulst, 1981, pp. 87, 98):

$$E(\theta) = \frac{a^4k^4l^2\bar{n}^4\left(\frac{n_c}{\bar{n}} - 1\right)^2(1+\cos^2\theta)}{8r^2}\overline{R^2(\theta)}E_0 \quad (5)$$

$$\text{with} \quad \overline{R^2(\theta)} = \frac{1}{z} \sum_{n=0}^{\infty} \frac{(-1)^n (2z)^{2n+1}}{(2n+1)\,(2n+1)!} - \left(\frac{\sin z}{z}\right)^2$$

$$\text{and} \qquad z = kl \sin\frac{\theta}{2}$$

with the values a, k, $\overline{n}$, and n_p as used in Eq. (4) and:

E_0 as the irradiance of the incident radiation (W/m^2),
$E(\theta)$ as the irradiance of the scattered radiation at the detector (W/m^2),
l as the length of the cylinder (crystal) = 160 nm,
n_c as the refractive index of the crystals = 1.651,
θ as the scattering angle, and
r as the distance from the scatterer to the detector (we used r = 1 m in this calculation).

In Fig. 1 (dashed line), the function $E(\theta) \cdot N_c/E_0$ (in m^{-3}) is shown.

The scattering cross-section of such a model crystal is given by the Rayleigh cross-section (van de Hulst, 1981, p. 68):

$$C_{sca} = \frac{a^4 k^4 l^2 \overline{n}^4 \pi}{6} \left| \left(\frac{n_p}{\overline{n}}\right)^2 - 1 \right|^2 \qquad (6)$$

Using the data previously given, we find $C_{sca} \simeq 1.4 \times 10^{-19}$ m^2. Note that C_{sca} is proportional to the square of the length of the model crystal.

Appendix 3. Calculation of the single-scattering properties of the prisms.

In the case of scattering by prisms, the conditions like those in Eq. (4) are not quite fulfilled here, but as an estimation of the forward-scattered radiation, we applied the Rayleigh-Gans theory. We must be aware that the prisms are not randomly oriented. As a model for the prisms, we used a circular cylinder, with radiation obliquely incident on it. The scattering intensity functions of such cylinders are given by (van de Hulst, 1981, pp. 87, 94):

$$E(\alpha,\varnothing,\theta) = \frac{a^4 k^4 l^2 \overline{n}^4 \left(\frac{n_p}{\overline{n}} - 1\right)^2 (1 + \cos^2\theta)}{8r^2} \left| R(\alpha,\varnothing,\theta) \right|^2 E_0$$

$$\text{with } R(\alpha,\varnothing,\theta) = \frac{2}{u} J_1(u) \left(\frac{\sin v}{v}\right),$$

$$u = 2ka \sin\frac{\theta}{2} \sin\beta, \; v = kl \sin\frac{\theta}{2} \cos\beta, \qquad (7)$$

$$\sin\beta = \left(\sin^2\alpha \sin^2\varnothing - (\sin\alpha \cos\varnothing \sin\tfrac{\theta}{2} + \cos\alpha \cos\tfrac{\theta}{2})^2\right)^{1/2},$$

$$\text{and } \cos\beta = \sin\alpha \cos\varnothing \cos\tfrac{\theta}{2} - \cos\alpha \sin\tfrac{\theta}{2}.$$

with:
a as the radius of the prism model = 2.5 µm,
l as the length of the prism model = 1 mm,
$\overline{n}_p$ as the refractive index of the prism = 1.619,
n as the refractive index of whole enamel = 1.616,
α as the angle between the cylinder axis and the incident direction,
θ as the scattering angle, and
$\varnothing$ as the angle between a plane through the cylinder axis and the incident direction (*i.e.*, the incident plane) and the scattering plane.

In Fig. 1 (solid line), the function $E(\theta) \cdot N_p/E_0$ (in m^{-3}) is shown, in which $E(\theta)$ is the average value for an ensemble of prisms oriented at angles α = 20°-90° and $\varnothing$ = 60°-90°.

To estimate the scattering cross-section, C_{sca}, of a single prism, we have to integrate the scattered radiation over all directions (van de Hulst, 1981, p 95):

$$C_{sca} = \frac{2 \int_{20°}^{90°} d\alpha \int_{0°}^{180°} d\varnothing \int_{0°}^{180°} d\theta \sin\theta \, E(\theta,\alpha,\varnothing)}{E_0 \int_{20°}^{90°} d\alpha} \qquad (8)$$

This results in $C_{sca} = 2.4 \times 10^{-10}$ m^2.

Appendix 4. Calculation of the Fraunhofer diffraction of prisms

Radiation perpendicularly incident on a regular grating of slits is Fraunhofer-diffracted. This radiation can be observed by placing a screen behind the grating. The normalized intensity function of the diffracted radiation is given by (Born and Wolf, 1980):

$$I(\theta) = N^2 \left(\frac{\sin(\frac{Nkd}{2}\sin\theta)}{N \sin(\frac{kd}{2}\sin\theta)}\right)^2 \qquad (9)$$

with:
d as the distance between the slits,
N as the number of slits, and
θ as the angle with the incident direction.

If the periodicity of the grating is a value with some variation, a wide first-order maximum and vanishing higher-order maxima will occur. The normalized intensity function of such an irregular grating can be calculated by the addition of diffraction patterns as given by Eq. (9), while using values of d that vary according to a normal distribution, with mean value d_{mean} and standard deviation σ_d. Adding such a sum of diffraction patterns to the angular intensity function arising from scattering without diffraction

$$P_3(\theta) = P_1(\theta) + C \sum_{n=0}^{5000} \left(\frac{\sin(\frac{Nkd_n}{2}\sin\theta)}{N \sin(\frac{kd_n}{2}\sin\theta)}\right)^2 \qquad (10)$$

with the previously used data and:
$P_3(\theta)$ as the total amount of transmitted light as a function of the scattering angle θ calculated in sector 2 (Fig. 3),
$P_1(\theta)$ as the total amount of transmitted light as a function of

the scattering angle θ measured in sector 1 (Fig. 3),
C as an arbitrary constant,
d_n as the periodicity of the grating, drawn, for every value of n, pseudo-randomly from a normal distribution, with a mean value d_{mean} and a standard deviation σ_d, and
N as the number of slits. (We took $N = 200$, being the ratio of the diameter of the laser beam $\simeq$ 1 mm and the expected periodicity $\simeq$ 5 μm.)

$P_3(\theta)$ was fit to $P_2(\theta)$, which was measured, the fit parameters being d_{mean} and σ_d.

If the slits are somewhat curved, the diffraction pattern will spread around the major direction of diffraction, as shown in Fig. 3. So, by measuring $P_w(\varnothing)$ in a window covering the first-order maximum, we can estimate the curvature of the prisms.